International Journal of Advanced Research and Interdisciplinary Scientific Endeavours, Vol. 3(2), 2025
DOI: 10.61359/11.2206-2543

# A Computational Journey of Hypersonic Phenomenon Travelling Towards the Aerospace Horizons and Beyond

Pradyumna Rangnath Surwase*

Email Correspondence*: pradyumnasurwase1999@gmail.com

M.Tech Aerospace, Ajeenkya D Y Patil University, Pune, Maharashtra, India.

**Abstract:**

This study provides an extensive analysis of hypersonic flow modeling and its applications, including scramjets and detonation phenomena. A computational analysis was conducted to compare the drag of two-dimensional re-entry vehicles: one with a blunt shape and the other with a wedge shape. Furthermore, the aerodynamic characteristics of the re-entry vehicles were investigated at various Mach numbers. These hypersonic simulations were evaluated using different turbulence models. To enhance thrust and specific impulse, the NASA Hyper X-43A scramjet shape was employed as a reference in the application section, with modifications made to the throat regions of the combustion chamber, which were scaled to 1.4 and 2.8 times, respectively. The fuel injectors used were two spike-shaped struts, and simulations were performed at various Mach numbers. Additionally, simulations of the exterior segment of the NASA Hyper X-43A scramjet vehicle were conducted. Subsequently, a single wedge-shaped fuel injector was utilized to examine the stability of detonation waves and to compare them to deflagration, thereby studying the detonation phenomenon.

**Keywords:** Scramjet, Detonation, Hypersonics, Rarefied Gas Dynamics, Fuel Injectors, Combustion, Knudsen Number, Re-Entry Vehicle.

## 1. Introduction

For computational analysis of any flow governing equations play a major role. Similarly for modelling of hypersonic flows, Navier-stokes equations are of primary concern. T. Chourushi.et al [1] proposed a paper on the computational analysis of flow near continuum by using the Navier-Stoke's equation. Christopher J. Roya et al [2] studied about modelling of hypersonic flows. But hypersonic phenomenon occurs at higher altitudes where density is low giving rise to rarefied gas dynamics. F. Sharipov et al [3] stated the importance of Rariefied gas dynamics by mentioning the Knudsen number. Shutian Yu et al [4] presented a method for the computational analysis of a biconic blunt re-entry vehicle. Iain D. Boyd et al [5] stated the Monte-Carlo method for the hypersonic flow simulation. Inorder to study hypersonic flows in deep, some applications are also included in Laurie A. Marshall et al [6] researched on the NASA X-43A scramjet engine. Recently, research was going on for efficient fuel mixing in the scramjet combustion. Sukanta Roga [7] presented a computational analysis on the diamond shaped struts for the parallel injection techniques of fuel in the combustion chamber. On the other hand, Jeong-Yeol Choia et al [8] presented research on the transverse injection techniques for the fuel in the combustion chamber. Kumari Ambe Verma et al [9] did computational analysis of combustion chamber over various angles of attack. Haomin et al [10] studied the effect the effect of combustion chamber geometry on thrust as well as specific impulse. et al Detonation phenomenon created revolution in the space propulsion. Gene P. Menees et al [11] studied about the oblique wave detonation. Piotr WolaĔski [12] gave an idea about the different types of detonation. [14]

*MTech Aerospace, Ajeenkya D Y Patil University, Pune, Maharashtra, India.

**Article Timeline: Received:** Jul 16, 2025; **Revised:** Aug 20, 2025; **Accepted:** Aug 30, 2025; **Published:** Aug 30, 2025

Daopeng Zheng et al gave an overview on how the turbojet engines got evolved. Daniel A. Rosatoa et al [15] explained the stabilized detonation in hypersonic propulsion. Zonglin Jiang et al [16] presented issues in the experimental analysis of detonation. Emerging hypersonic airbreathing propulsion systems promise to revolutionize flight by enabling new vehicle types that offer rapid response, long range, and enhanced maneuverability, with reliable access to space. Traditionally, hypersonic vehicles, moving faster than five times the speed of sound, have used rocket boosters, but new developments focus on achieving sustained hypersonic flight using airbreathing engines like turbojets, ramjets, scramjets, and dual-combustion ramjets (DCRs), which capture atmospheric oxygen and use conventional fuels. While turbojets are limited to speeds around Mach 3.5 and ramjets face limitations above Mach 5, scramjets work efficiently at hypersonic speeds, and DCRs and turbo-ramjets offer broader operational ranges. Recent advances indicate that operational hypersonic systems capable of reaching speeds up to Mach 6 with conventional fuels are becoming feasible, enhancing the potential for high-performance, versatile hypersonic vehicles.

## 2. Methods

Modelling of hypersonic flows and studying the computational analysis of their application was the aim of this work. The scope of modeling hypersonic flows encompasses the study of fluid dynamics at extremely high velocities, typically exceeding Mach 5. These flows exhibit complex phenomena, including shock waves, boundary layer interactions, chemical reactions, and high-temperature effects resulting from aerodynamic heating. Accurate modeling necessitates advanced computational fluid dynamics (CFD) techniques that incorporate real gas effects, turbulence modeling, and thermodynamic non-equilibrium. Hypersonic flow models have critical applications in aerospace engineering, particularly in the design of re-entry vehicles, space shuttles, hypersonic missiles, and air-breathing propulsion systems such as scramjets. These technologies are essential for space exploration, defense systems, and next-generation transportation solutions. All the simulations were carried out at computer lab in Ajeenkya D Y Patil University.

## 3. Problem Statement

There are three sections to this study project. In the first section, computational research was done on a variety of 2D re-entry vehicle designs, including wedge and blunt shapes, to compare the drag. To compare the outcomes, they were also simulated across a range of turbulence models. Additionally, the re-entry vehicles were simulated at different Mach numbers. The internal engine geometry and external vehicle of the NASA X-43A scramjet are included in the second section. The reference [14] was followed in altering the internal engine shape. To do the computational analysis at different angles of attack and mach numbers, two aerospike-shaped fuel injectors were utilized. The goal was to find a design that would yield optimal results for effective fuel mixing. The identical geometry from the second section was used in the third portion, however this time a computer analysis was performed for detonation. An individual wedge-shaped fuel injector was employed to verify the detonation waves' stability analysis.

## 4. Computational Model

According to reference [15] the phenomenon known as turbulence mostly manifests at higher Reynolds numbers. A variety of simulation techniques, including large-eddy simulation (LES) and direct numerical simulation (DNS), are commonly used. Larger length scales are primarily employed for modeling turbulent flows, with the LES method being less expensive than the DNS method. The Reynolds Averaged Navier Stokes (RANS) model, however, yields the best outcomes as it can work with all kinds of length scales. The computational analysis in this paper utilizes the Spalart-Almaras one-equation model, one of the many solvers available. Other solvers include two-equation solvers like k-epsilon and k-w. RANS solvers are primarily used for optimizing aerodynamic performance in aircraft and turbomachinery. They can also be applied in off-design scenarios such as boundary layer separation and boundary layer shockwave interaction

modeling. Therefore, the RANS modeling approach was employed for simulating the flow phenomenon around re-entry vehicles.

The governing equations for RANS modeling are :

$$\frac{\partial \rho}{\partial x} + \frac{\partial}{\partial x}(\nabla . \rho V) = 0 \quad \textbf{(10)}$$

$$\frac{\partial}{\partial t}(\rho u_i) + \frac{\partial}{\partial x_j}(\rho u_i u_j) = -\frac{\partial P}{\partial x} + \frac{\partial}{\partial x_j}(|\rho \mu \frac{\partial u_i}{\partial x_j})| \quad \textbf{(11)}$$

The development of accurate transport models is crucial for simulating hypersonic combustion, a complex phenomenon characterized by high-speed flows and intense heat transfer. Various models have been proposed to capture the underlying physics, including the Navier-Stokes equations with finite-rate chemistry (NS-FRC), Reynolds-Averaged Navier-Stokes (RANS) equations with turbulence-chemistry interaction (TCI), and Large Eddy Simulation (LES) with sub grid-scale (SGS) modeling. A critical evaluation of these models reveals that each has its strengths and limitations, with NS-FRC being suitable for lower Mach numbers, while RANS-TCI and LES-SGS are more applicable to high-Mach number flows.

### 4.1.1 Geometry

A wedge geometry of 20m*20m (base and height) was chosen for the analysis. A rectangular domain of 250m*150m was chosen in which wedge was placed at 65 m from both the upper and lower fairfield. On the other hand, the wedge was at a distance of 90m from the inlet and 160m from the outlet. Face meshing was done for the wedge with element size of 0.1 m and the overall meshing was done by taking the 0.75m size of each element. The total number of nodes was 70355 and the total number of cells was 69548. The named selections were inlet, outlet and ff1, ff2.

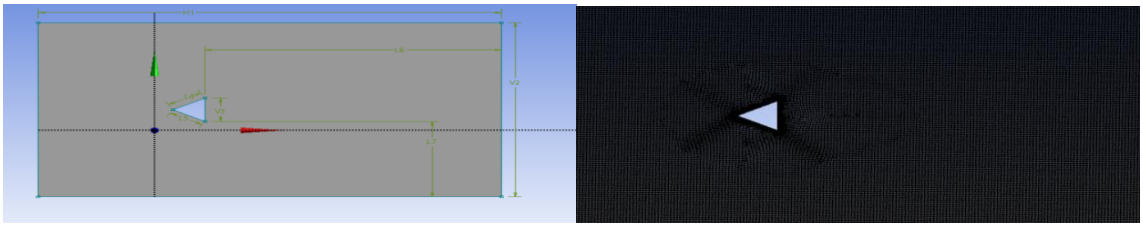

**(a) Geometry of wedge shaped 2D re-entry vehicle** **(b) Meshing of wedge shaped 2d re-entry vehicle**

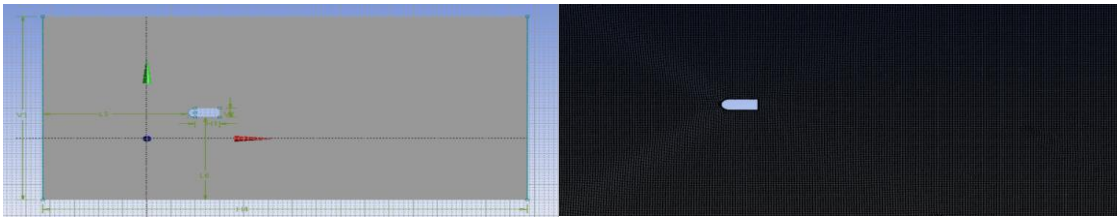

**(c) Geometry of a bluff body without spike** **(d) Mesh of bluff body with spike**

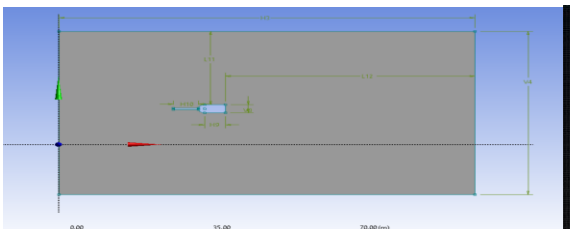

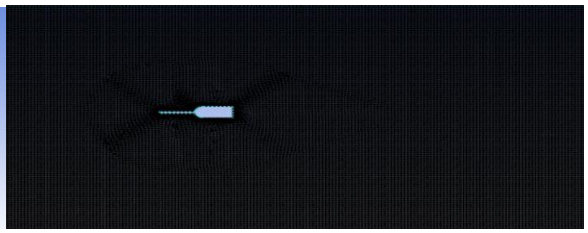

**(e) Geometry of a bluff body with spike** **(f) Mesh of bluff body with spike**

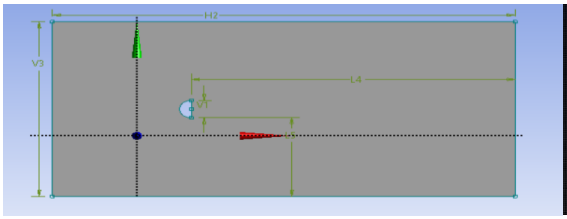

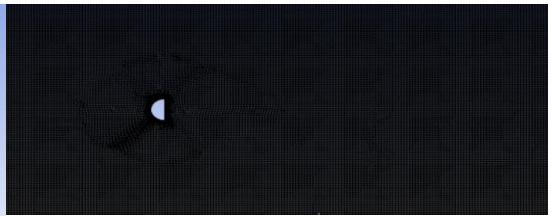

**(g) Geometry of a blunt body** **(h) Meshing of a bluff body**

**Figure 1: Geometry of different shapes of 2D re-entry vehicles**

**Table 1: Dimensions of internal scramjet geometry**

| Scramjet Section | Inlet Nozzle | Throat | Outlet of Isolator | Outlet of 1st section of C.C. | Outlet of 2nd section of isolator | Exhaust |
|---|---|---|---|---|---|---|
| Area ($m^2$) | 0.4095 | 0.2426 | 0.2426 | 0.3397 | 0.67 | 0.9 |

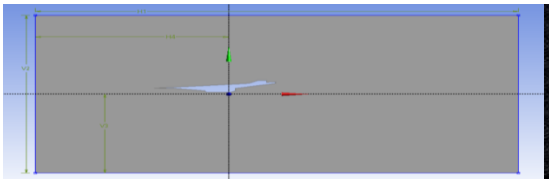

**(a)Geometry of NASA X-43A Scramjet Vehicle Vehicle** **(b) Meshing of NASA X-43A Scramjet**

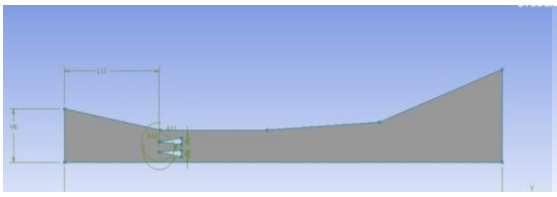

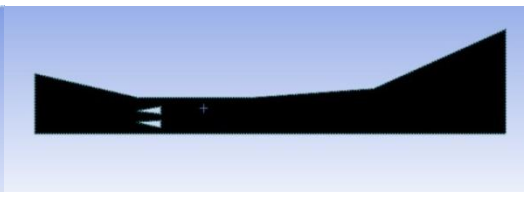

**(c) Geometry of internal scramjet geometry of NASA X-43 A**

**(d) Mesh of internal scramjet geometry of NASA X-43 A**

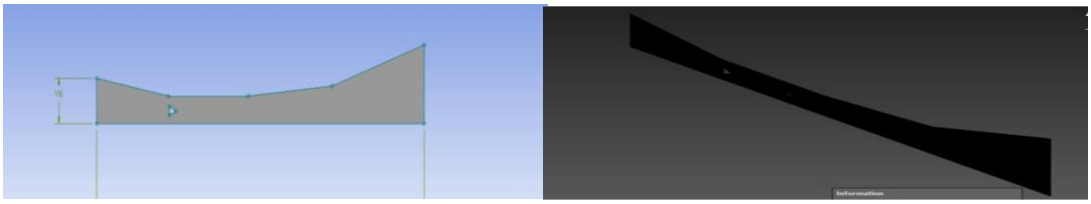

**(e)Geometry of rnal scramjet geometry of NASA X-43 A for detonation**

**(f) Meshing of rnal scramjet geometry of NASA X-43 A for detonation**

**Figure 2: Model of scramjet for combustion and detonation**

### 4.8.3 Pre-processing

**For re-entry vehicles and external scramjet vehicles**

The simulation was carried out by using the pressure based solving approach as the incoming flow is subsonic. The energy equation was also used for calculating the temperature. The realizable k-epsilon model was used as it was more accurate than other models. The incoming gas was chosen to be ideal gas whose density varied along with the Sutherland law. The residual value was set up to 10^-6. The coupled method was used along with the second order scheme for spatial discretization's like pressure, density, momentum, turbulent kinetic energy, turbulent dissipation rate and energy. A global time step method was used for the computation along with the least squares method. 1000 iterations were performed to achieve the 10^-6 value of the scaled residuals for converging the solution

**For scramjet combustion and detonation**

A simple approach was followed for the computational analysis of the scramjet. First a density-based approach was selected by selecting the energy equation along with double temperature model. The k-epsilon realizable turbulence model was selected for the analysis. The incoming air was chosen to be an ideal gas, and viscosity was kept tpo vary with Sutherland's Law. The boundary conditions were chosen according to the below mentioned table. Spatial discretization methods were chosen to be Implicit, along with the AUSM Scheme. All other schemes were chosen to be third order MUSCL. The residuals were set to be 10^-6 and the solution was initialized standardly from inlet.

**Table 2: Boundary Conditions of internal modified scramjet geometry of NASA X-43 A hyper scramjet**

**Boundary Conditions**

For internal scramjet combustion and detonation

| **Boundary Name** | Inlet | Far Field | Fuel Injectors | Outlet |
|---|---|---|---|---|
| **Boundary Type** | Pressure farfield | Wall | Pressure farfield | Pressure farfield |
| **Boundary Conditions** | M=5,7.5,10<br>P= 0 Pa<br>T= 300 K | No slip | M=1,2,3<br>P= 0 Pa<br>T= 300 k | M=0.6<br>P = 0 Pa<br>T= 300 K |

**Table 3: Species mole fraction for inlet air**

| **Species** | $O_2$ | $N_2$ | $H_2O$ | $H_2$ |
|---|---|---|---|---|
| **Mole fraction** | 0.232 | 0.736 | 0.032 | 0 |

**Table 4: boundary conditions for NASA x-43 a scramjet vehicle**

| **Boundary Name** | Inlet | Farfield | Outlet |
|---|---|---|---|
| **Boundary Type** | Velocity Inlet | Wall | Pressure Outlet |
| **Boundary Conditions** | Mach no 5<br>Gaugage pressure 0<br>Temperature 300k<br>Turbulent intensity 10% | Wall conditions | Outlet guage pressure<br>Temperature 300k<br>Turbulence intensity 10% |

## 5. Results

The simulation was carried out by using the pressure based solving approach as the incoming flow is subsonic. The energy equation was also used for calculating the temperature. The realizable k-epsilon model was used as it was more accurate than other models. The incoming gas was chosen to be ideal gas whose density was varying along with the sutherland law. The inlet boundary condition was set as 0.58 mach number. The residual value was set up to 10^-6. The coupled method was used along with the second order scheme for spatial discretization's like pressure, density, momentum, turbulent kinetic energy, turbulent dissipation rate and energy. A global time step method was used for the computation along with the least squares method. 1000 iterations were performed to achieve the 10^-6 value of the scaled residuals for converging the solution.

The simulation was carried out by using the pressure based solving approach as the incoming flow is subsonic. The energy equation was also used for calculating the temperature. The realizable k-epsilon model was used as it was more accurate than other models. The incoming gas was chosen to be ideal gas whose density was varying along with the sutherland law. The inlet boundary condition was set as 0.58 mach number. The residual value was set up to 10^-6. The coupled method was used along with the second order scheme for spatial discretization's like pressure, density, momentum, turbulent kinetic energy, turbulent dissipation rate and energy. A global time step method was used for the computation along with the least squares method. 1000 iterations were performed to achieve the 10^-6 value of the scaled residuals for converging the solution.

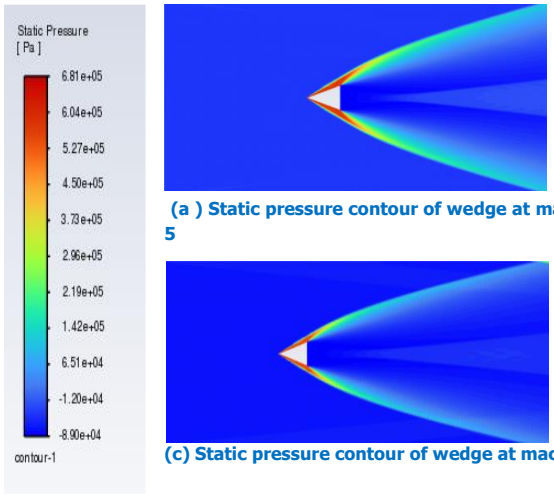


(a ) Static pressure contour of wedge at mach 3 5

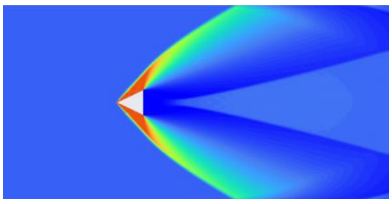

(b) Static pressure contour of wedge at mach



(c) Static pressure contour of wedge at mach 8

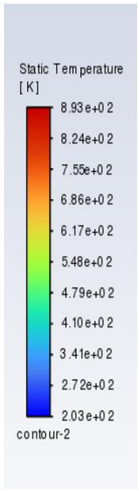


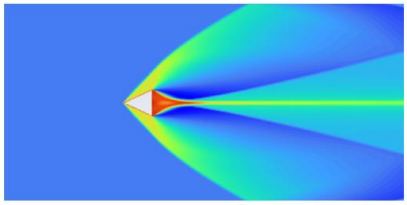

(a) Static temperature contour of wedge at mach 3

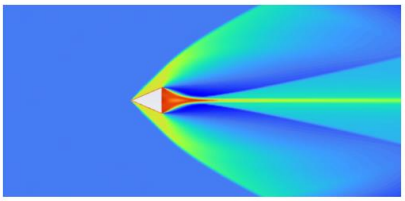

(b) Static temperature contour of wedge at mach 5

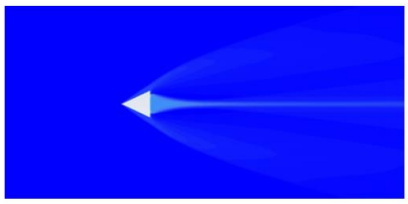

(c) Static temperature contour of wedge at mach 8

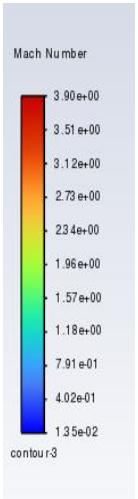


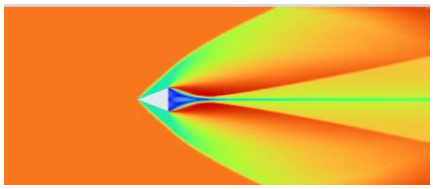

(a) Mach number contour of wedge at mach 3

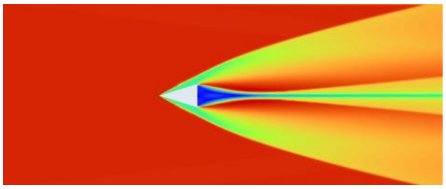

(b) Mach number contour of wedge at mach 5

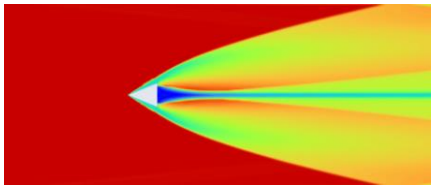

(c) Mach number contour of wedge at mach 8

**Figure 3: Comparison of static pressure contours at various angles of attack**

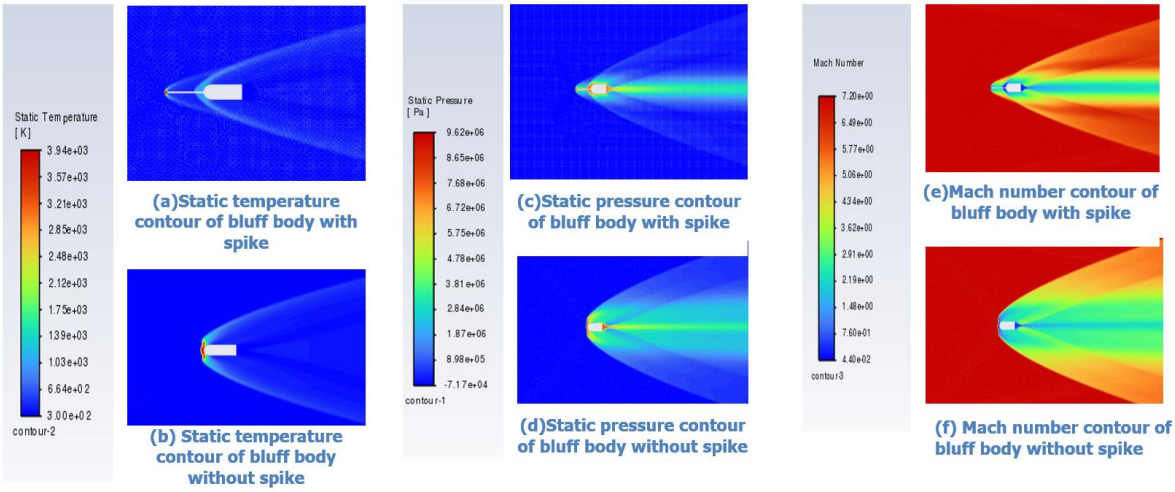


**Figure 4: Comparison of static temperature, static pressure and mach number contours for re-entry vehicles having bluff body with spike and without spike**

## 6. Observations

At Mach number 5, the wedge-shaped re-entry vehicle generates two oblique shock waves at its apex, accompanied by two expansion fans at the base vertices. These shock waves cause a decrease in Mach number, resulting in an increase in pressure and temperature. This change is visually represented by a transition from a higher Mach number (depicted in red) to a lower Mach number (depicted in lighter green). On the other hand, the expansion fans cause an increase in Mach number, leading to a reduction in pressure and temperature. This transformation is illustrated by a transition from a light green shade back to red. Additionally, the presence of vortices and wake-like structures at the base of the wedge creates a region of lower Mach number, represented by the color blue. Similar changes in pressure and temperature can be observed in different colors.

In the case of a blunt body, a bow shock forms at the frontal section, unlike the two oblique shocks in a wedge structure. However, all other phenomena remain consistent with the wedge configuration. For a bluff body, a bow shockwave emerges along with three smaller spherical wavefronts at the frontal extremity. In simulations involving a bluff body with a spike, an initial normal shockwave appears in front of the spike, followed by the formation of a bow shock at the forefront of the bluff body. The interaction between the normal shock and bow shock further reduces the flow velocity, resulting in a decrease in the drag coefficient. Comparative analysis shows that as the Mach number increases; the drag coefficient of the wedge-shaped re-entry vehicle decreases. Furthermore, a comparison between a bluff body without a spike and one with a spike indicates a decrease in drag**.** An external geometry of NASA X-43A Hyper scramjet vehicle was simulated at mach 5 and different angles of attack 0, 5, and 10. All major parts of external geometry of scramjet were producing the shocks including inlet leading edge, engine intake, rudder and elevator. The leading edge was producing oblique shock which was weak. The shock interaction was happening in between rudder and elevator shocks. A region of high temperature was produced starting from the tail section.

The static temperature contours showed that the temperature was maximum around the scramjet, and it decreased as the distance from the scramjet was decreased. This was shown by the red coloured layer followed by a light green coloured layer around the scramjet. One light green coloured layer starting from the engine intake went downwards with the diminishing intensity. This was due to the shock occurred due to the nozzle inlet shape which increased the pressure of incoming flow. Similar phenomenon had occurred for the shock produced around the rudder. The mach number contours also showed the shocks occurred

due to the engine inlet and rudder. In addition to this, it also shows a weak oblique shockwave at the tip of the scramjet vehicle. But, after angle of attack 10 degrees it diminished. The yellow-coloured region in the mach number contour at 10 degrees shows the formation of region like the stagnation region having lower velocity. It also showed that the nozzle inlet and the rudder shocks were nullified. As the angle of attack was increased, the thickness of the red layer around the vehicle increased, which showed the increase of heat. This also represents increase in drag. Also, the temperature distribution from the 10 degrees angle of attack was changed to concentric circles for each zone.

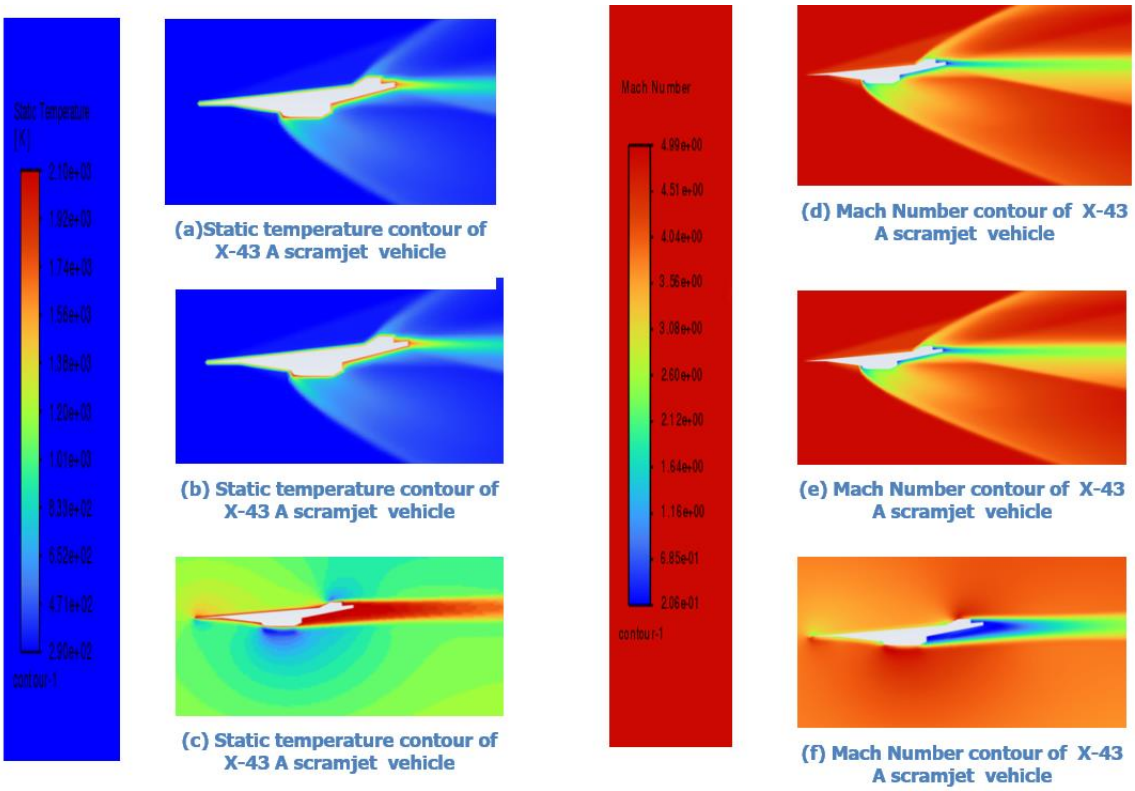


**Figure 5: Comparison of contours of static temperature and mach number for external scramjet X-43 A vehicle**

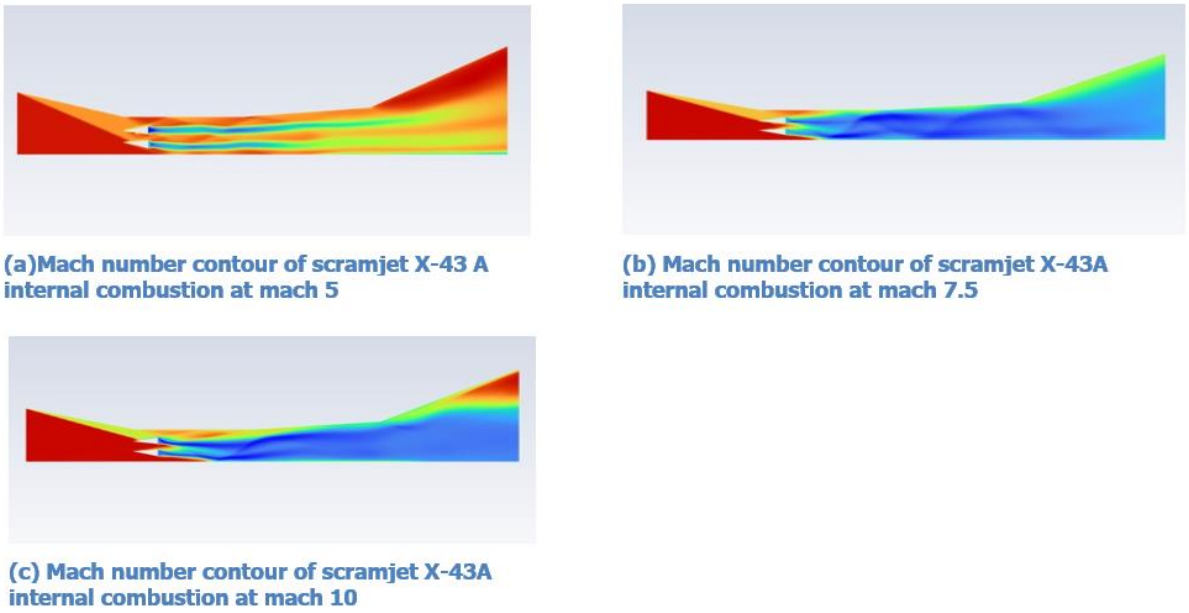

(a)Mach number contour of scramjet X-43 A internal combustion at mach 5

(b) Mach number contour of scramjet X-43A internal combustion at mach 7.5

(c) Mach number contour of scramjet X-43A internal combustion at mach 10

**Figure 6: Comparison of mach number contour of scramjet internal combustion by varying mach number**

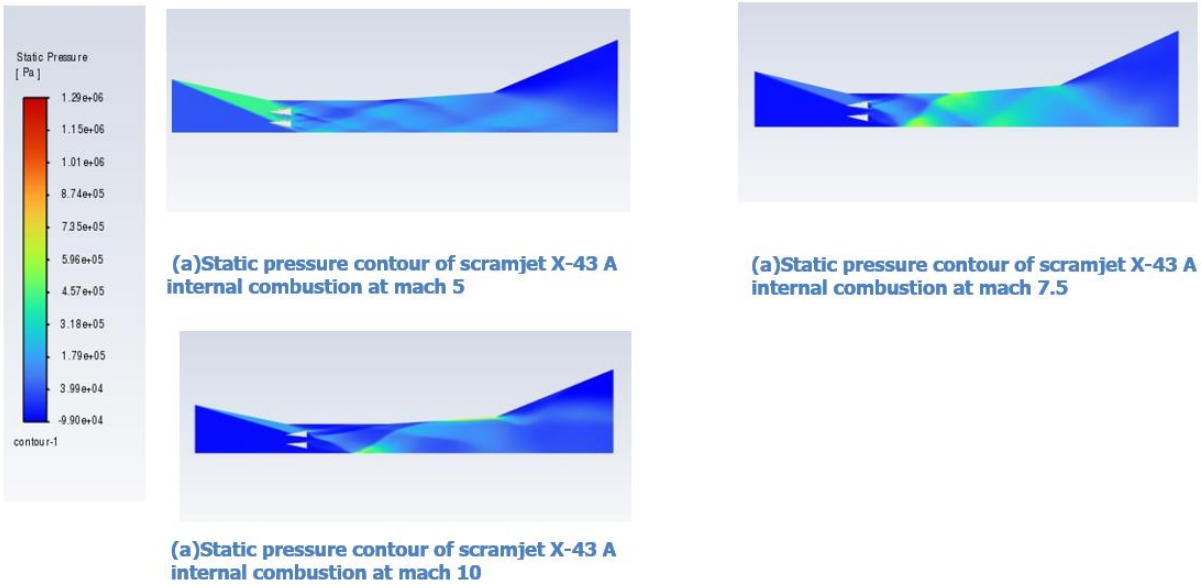


(a)Static pressure contour of scramjet X-43 A internal combustion at mach 5

(a)Static pressure contour of scramjet X-43 A internal combustion at mach 7.5

(a)Static pressure contour of scramjet X-43 A internal combustion at mach 10

**Figure 7: Comparison of static pressure contour of scramjet internal combustion by varying mach number**

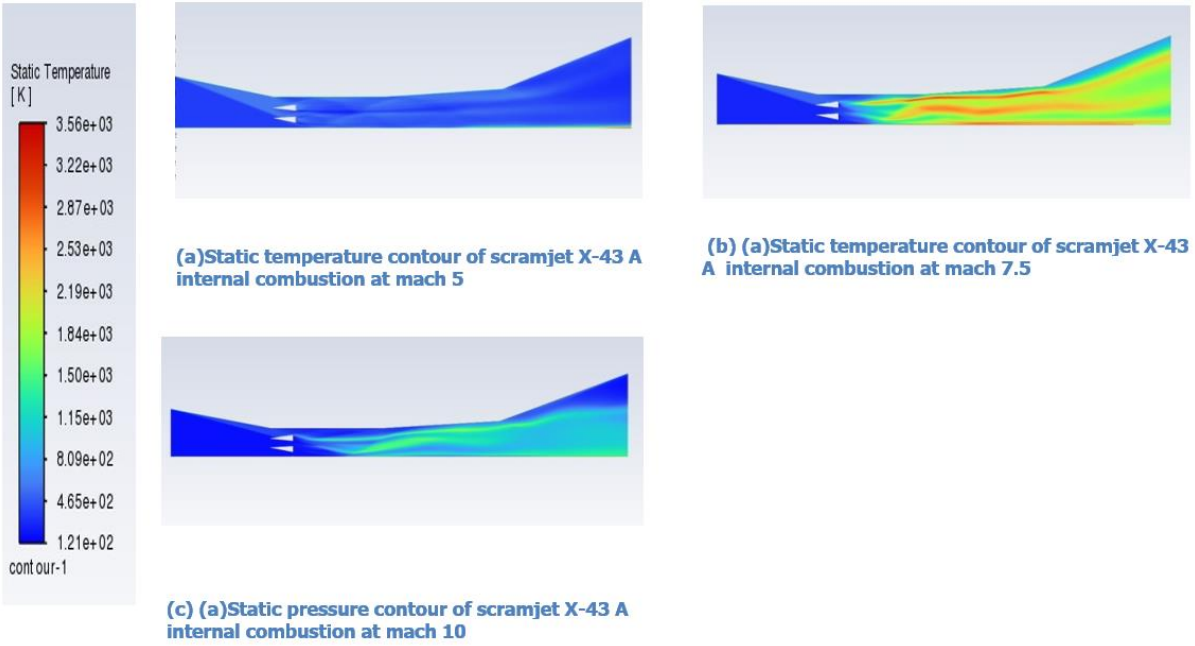


**Figure 8: Comparison of static temperature contour of scramjet internal combustion by varying mach number**

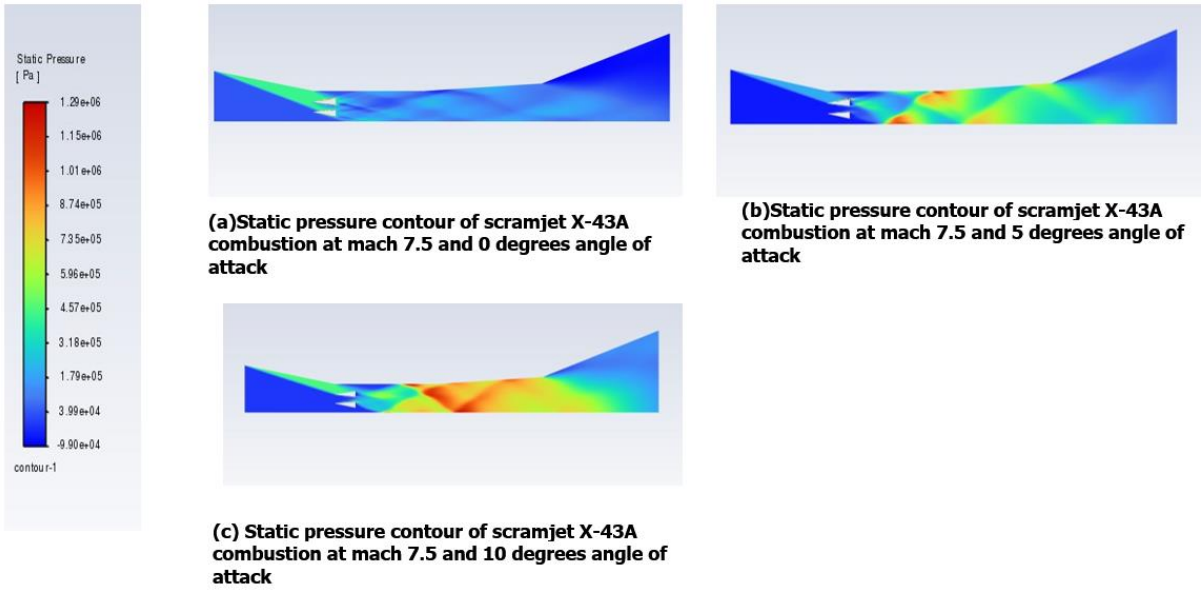


**Figure 9: Comparison of static temperature contour of scramjet internal combustion by varying mach number as well as angle of attack**

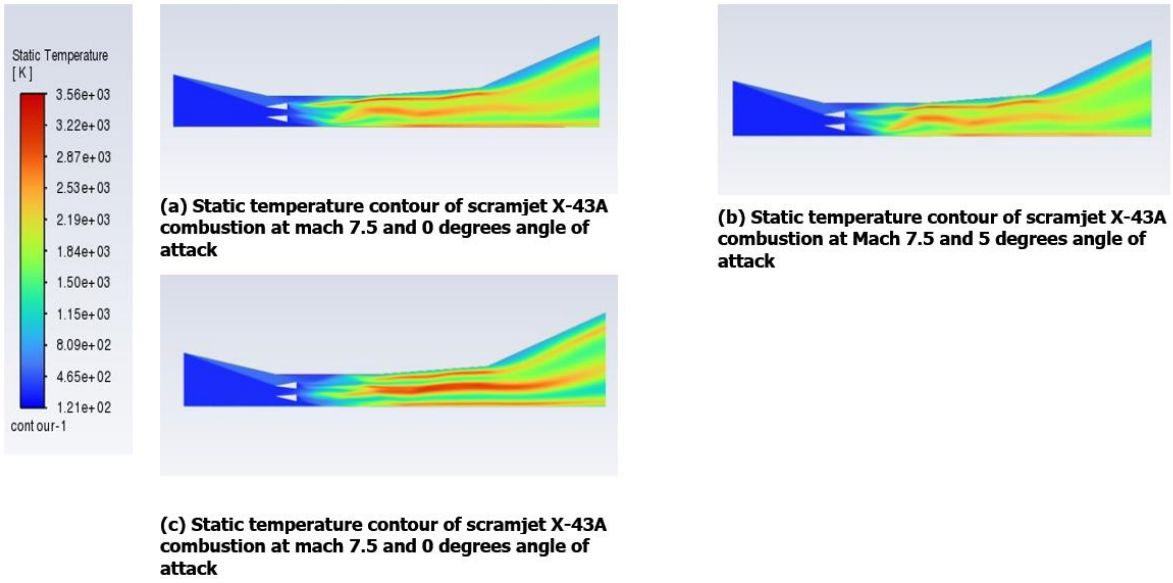


**(a) Static temperature contour of scramjet X-43A combustion at mach 7.5 and 0 degrees angle of attack**

**(b) Static temperature contour of scramjet X-43A combustion at Mach 7.5 and 5 degrees angle of attack**

**(c) Static temperature contour of scramjet X-43A combustion at mach 7.5 and 0 degrees angle of attack**

**Figure 10: Comparison of static pressure contour of scramjet internal combustion by varying mach number as well as angle of attack**

When air came inside the combustion chamber through the inlet of a scramjet engine, it produced oblique shocks due to striking on the aerospike shaped fuel injectors. These shocks then reduced the speed of the incoming flow and due to the shock and boundary layer interaction the fuel was mixed with the incoming air effectively. As the mach number was increased the number of reflections of the shocks of incoming air were reduced. This was because the increased mach number causes increase in the speed of the incoming air which causes less time of air to have interaction with fuel in the combustion chamber. Hence, the efficiency of mixing of fuel with the air decreases. The static temperature contours showed that the temperatures of the flames were increased after the mixing of fuel with the air due to the shockwave boundary layer interaction. The mach number of the fuel was lesser as compared to the incoming air . As the flow goes ahead, the mach number increased due to the mixing of fuel with air but, it decreased at the regions were shockwave interacted with the flame. At the last, the intensity of shocks was diminished and the mach number of the flame was increased. As the angle of attack of the injection of fuel was increased, the fuel was mixed with the air more efficiently along with the decrease in speed and increased pressure regions were formed. With the increasing angle of attack the flame was spread more in the combustion chamber. Increasing mach number also increases the thickness of thermal boundary layer along with increased temperature of flame.

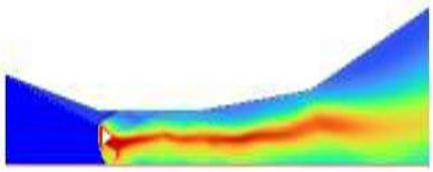

(a) Static Temperature Contour of internal scramjet at Mach 10 and angle of attack 5 degrees

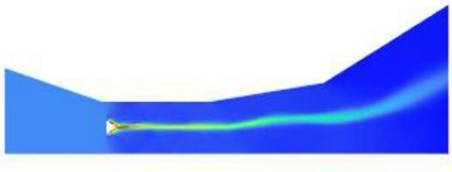

(c) Static temperature Contour of internal scramjet at Mach 5

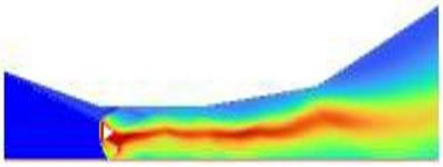

(b) Static Temperature Contour of internal scramjet at Mach 10 and angle of attack 10 degrees

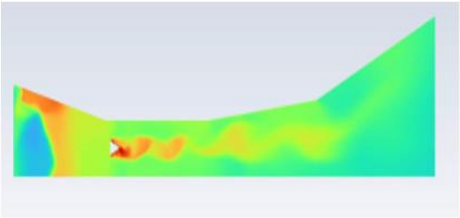

(d) Static temperature Contour of internal scramjet at Mach 10

**Figure 11: Comparison of static temperature contours of detonation by varying mach number as well as angle of attack**

(a) Static pressure Contour of internal scramjet at Mach 5

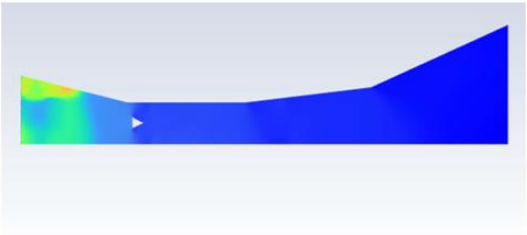

(b) Static pressure Contour of internal scramjet at Mach 10

(c) Static pressure Contour of internal scramjet at Mach 10 and angle of attack 5 degrees

(d) Static pressure Contour of internal scramjet at Mach 10 and angle of attack 10 degrees

**Figure 12: Comparison of static pressure contours by varying mach number as well as angle of attack for detonation**

A detonation wave preceding the isolator segment exhibited a velocity lower than that of the flow within the isolator segment, thereby serving to avert the occurrence of an upstream shockwave and the consequent unstart of the engine. The stability of detonation waves was assessed subsequent to the

computational scrutiny of a scramjet featuring a solitary fuel injector. The simulations entailed the alteration of the Mach numbers to 5 and 10, alongside the substitution of hydrogen with diverse fuel ethanol. Furthermore, the assessment of stability involved the variation of angles of attack up to 5 and 10 degrees. Upon reaching an Angle of Attack (AOA) of 10 degrees, it was observed that the pressure attained its peak subsequent to the flow impacting the fuel injector wall. The pressure then commences a decline as the flow transitions in an upward trajectory, coinciding with the maximum temperature post the formation of a shockwave at the wall's surface. With an escalation in the Mach number, a reduction in the thickness of the detonation wave was noted. Additionally, the utilization of ethanol as a fuel source led to the observation of an asymmetrical detonation wave, characterized by the presence of two minor bow shocks. Moreover, an increase in the angle of attack resulted in an upward inclination of the detonation wave.

## 7. Future Scope

The future scope of modeling hypersonic flows is expanding due to advancements in innovative aerospace designs and technologies. For blended wing body re-entry vehicles, hypersonic flow modeling will facilitate optimized aerodynamics, stability, and thermal management, thereby enhancing re-entry performance and fuel efficiency. Bioinspired thermal protection systems present a promising avenue, as flow models can simulate heat transfer and thermal stresses to develop materials that emulate biological structures, improving the durability of re-entry vehicles under extreme heat conditions. In the context of 3D scramjets, advanced computational fluid dynamics (CFD) models will investigate various fuel injection strategies, taking into account cavities and optimizing combustion chamber geometry to enhance fuel-air mixing and combustion efficiency. Finally, modeling different types of detonations, including rotating and oblique detonation waves, will be crucial in developing more efficient propulsion systems for hypersonic vehicles, paving the way for breakthroughs in speed and fuel economy for space exploration and defense technologies.

## 8. Conclusion

**Modeling hypersonic flows and their practical implications have revealed several key findings:**

The increase in Mach number was found to correspond to an escalation in the drag experienced by re-entry vehicles. Moreover, the configuration of these vehicles played a crucial role in determining the nature of shock waves surrounding them. Specifically, wedge-shaped re-entry vehicles were associated with oblique shocks at their apex, while blunt-shaped ones exhibited bow shocks. In addition, it was observed that a bluff body featuring a spike generated less drag compared to a spikeless counterpart. The verification of the external geometry of the NASA X-43 A Hyper scramjet vehicle facilitated an in-depth exploration of external flow patterns around the craft. Furthermore, it was noted that the efficiency of fuel mixing within the combustion chamber of the internal scramjet varied inversely with Mach number but directly with the angle of attack. Computational analysis focusing on the stability of detonation waves highlighted that alterations in fuel composition led to changes in the shape of the detonation wave. Additionally, modifications in the bow structure of the detonation wave were observed, with a tendency for it to lean more towards an upward orientation.

## 9. Availability of Data and materials

Ryan J. Clark S. O. Bade Shrestha Detonation Combustion Wave Stabilization in Scramjets

August 2015 DOI: 10.2514/6.2015-4595 Conference: AIAA SPACE 2014 Conference and Exposition

Laurie A. Marshall* and Griffin P. Corpening† Robert Sherrill‡ A Chief Engineer's View of the NASA X-43A Scramjet Flight Test NASA Dryden Flight Research Center, Edwards, California, 93523-0273, USA

Hao-min Li, Yu-chun Chen, Chun Guan, Yuan Gao, Zhi-hua Wang, Yu-sang L Research on Geometry Configuration/Fuel Distribution of Combustion Chamber of Scramjet 2018 9th International Conference on Mechanical and Aerospace Engineering

## 10. Author's Contribution

This manuscript is written by Pradyumna Rangnath Surwase. All the simulations were carried out by him. Dr. Prashant Kumar has guided him.

## 11. Acknowledgement

I want to express my gratitude to Satya Sandeep C sir for his guidance and motivation towards completion of this project and Shiva Prasad Uppu sir for suggesting topic of aerospike shaped two fuel injectors for scramjet combustion.

## 12. References

[1] Chourushi, T., Rahimi, A., Singh, S., & Myong, R. S. (2020). Computational simulations of near continuum gas flow using Navier–Stokes–Fourier equations with slip and jump conditions based on the modal discontinuous Galerkin method. *Advances in Aerodynamics, 2*(8). https://doi.org/10.1186/s42774-020-00032-z

[2] Roy, C. J., & Blottner, F. G. (2006). Review and assessment of turbulence models for hypersonic flows. *Progress in Aerospace Sciences, 42*(6), 469–530.

[3] Sharipov, F. (2000). *Rarefied gas dynamics and its applications to vacuum technology.* Universidade Federal do Paraná.

[4] Yu, S., Ni, X., & Chen, F. (n.d.). CFD simulation strategy for hypersonic aerodynamic heating around a blunt biconic. *International Journal of Aerospace Engineering.*

[5] Boyd, I. D. (2015). Computation of hypersonic flows using the direct simulation Monte Carlo method. *Journal of Spacecraft and Rockets, 52*(1), 1–14. https://doi.org/10.2514/1.A32767.

[6] Marshall, L. A., Corpening, G. P., & Sherrill, R. (2005). A chief engineer's view of the NASA X-43A scramjet flight test. *NASA Dryden Flight Research Center, Edwards, California.*

[7] Das, N., Pandey, K. M., & Sharma, K. K. (2019). A brief review on the recent advancement in the field of jet engine – scramjet engine. *Materials Today: Proceedings.*

[8] Roga, S. (2019). CFD analysis of scramjet engine combustion chamber with diamond-shaped strut injector at flight Mach 4.5. *Journal of Physics: Conference Series, 1276,* 012041. https://doi.org/10.1088/1742-6596/1276/1/012041

[9] Choi, J.-Y., Ma, F., & Yang, V. (2005). Combustion oscillations in a scramjet engine combustor with transverse fuel injection. *Proceedings of the Combustion Institute, 30*(2), 2851–2858.

[10] Li, H., Chen, Y., Guan, C., Gao, Y., Wang, Z., & Yu, Y. (2018). Research on geometry configuration/fuel distribution of combustion chamber of scramjet. In *Proceedings of the 9th International Conference on Mechanical and Aerospace Engineering.*

[11] Verma, K. A., Pandey, K. M., Ray, M., & Sharma, K. K. (2020). Numerical investigation of combustion performance of scramjet combustor with variation in angle of attack. *Results in Engineering.*

[12] Menees, G. P., Adeleman, H. G., & Cambier, J.-L. (1995). Analytical and experimental investigations of the oblique detonation wave engine concept. *NASA Technical Reports.*

[13] Wolański, P. (2011). Detonation engines. *Journal of KONES Powertrain and Transport, 18*(3), 515–526.

[14] Zheng, D. (2024). Evolution of engines: From steam to turbojet. In *Proceedings of the 3rd International Conference on Computing Innovation and Applied Physics.*. https://doi.org/10.54254/2753-8818/31/20241149

[15] Rosato, D. A., Thornton, M., Sosa, J., Bachman, C., Goodwin, G. B., & Ahmed, K. A. (2024). Stabilized detonation for hypersonic propulsion. *Proceedings of the National Academy of Sciences.* https://www.pnas.org

[16] Jiang, Z., Zhang, Z., Liu, Y., Wang, C., & Luo, C. (2020). Criteria for hypersonic airbreathing propulsion and its experimental verification. *Chinese Journal of Aeronautics, 34*(2), 281–291. https://doi.org/10.1016/j.cja.2020.11.001

[17] Clark, R. J., & Shrestha, S. O. B. (2015, August). Detonation combustion wave stabilization in scramjets. In *AIAA SPACE 2014 Conference and Exposition.* https://doi.org/10.2514/6.2015-4595

[18] Yusof, S. N. A., Asako, Y., Sidik, N. A. C., Mohamed, S. B., & Japar, W. M. A. A. (2020). A short review on RANS turbulence models. *CFD Letters, 12*(11), 83–96.
[19] Zhang, Y., & Shen, H. (2020). Assessment of transport models for hypersonic combustion. *Journal of Propulsion and Power, 36*(3), 537–548.
[20] Surwase, P. R. (2024). Understanding turbulent flows and combustion in scramjets and hypersonic vehicles: A comprehensive review. *International Journal of Science and Research, 13*(9), 260–263. https://www.ijsr.net/getabstract.php?paperid=ES24902174720
[21] Mathews, R. N., & Shafeeque, A. P. (2015). Hypersonic flow analysis on an atmospheric re-entry module (blunt body). *International Journal of Engineering Research and General Science, 3*(5).
[22] Reddy, D. S. K., & Sinha, K. (2009). Hypersonic turbulent flow simulation of FIRE II reentry vehicle afterbody. *Journal of Spacecraft and Rockets, 46*(4), 753–762.
[23] Zore, K., Ozcer, I., Munholand, L., & Stokes, J. (2020). ANSYS CFD simulations of supersonic and hypersonic flows. In *Proceedings of the 6th National Symposium on Shock Waves (NSSW-2020).* IIT Madras.
[24] Del Corso, J. A., Cheatwood, F. M., Bruce, W. E., Hughes, S. J., & Calomino, A. M. (2018). Advanced high-temperature flexible TPS for inflatable aerodynamic decelerators. *American Institute of Aeronautics and Astronautics (AIAA).*
[25] Van Wie, D. M., D'Alessio, S. M., & White, M. E. (2005). Hypersonic airbreathing propulsion. *Johns Hopkins APL Technical Digest, 26*(4).
[26] Prasad, S. U., & Srinivas, G. (2012). Flow simulation over re-entry bodies at supersonic and hypersonic speeds. *International Journal of Engineering Research and Development, 2*(4), 29–34.
[27] Santosh, K., Prasad, S. U., Srinivas, G., & Manikandan, M. (2012). Computational analysis of hypersonic flow field over re-entry bodies. *International Journal of Systems, Algorithms & Applications, 2*(ICASE 2012), 1–6.

## 13. Conflict of Interest

The author declares no competing conflict of interest.

## 14. Funding

No funding was issued for this research.